NONLINEAR AERODYNAMIC DAMPING OF BEAMS AT HIGH OSCILLATORY REYNOLDS NUMBERS

Rahul A. Bidkar, Mark Kimber, Arvind Raman, Anil K. Bajaj & Suresh V. Garimella
School of Mechanical Engineering & Birck Nanotechnology Center
Purdue University, West Lafayette, IN 47907, USA.

ABSTRACT

Slender, sharp-edged flexible beams commonly found in aeronautical and electronics cooling applications as well as in biological structures often undergo oscillations with amplitudes comparable to their widths. Under these conditions, the structural oscillation in the surrounding quiescent fluid gives rise to damping forces which vary nonlinearly with the structural motion. In this article, we experimentally demonstrate the phenomenon of nonlinear, amplitude-dependent *aerodynamic damping of slender piezoelectric fans oscillating in a surrounding fluid at moderately high Reynolds numbers. We then develop a theoretical model using an Euler-Bernoulli beam coupled to an inviscid, incompressible fluid with allowance for separation and vortex-shedding from the beam's sharp edges. The theoretical model developed here successfully predicts the experimentally measured aerodynamic damping and its dependence on the structural oscillation amplitude.*

1. INTRODUCTION AND BACKGROUND

The presence of a surrounding fluid significantly modifies the dynamics of oscillating slender, sharp-edged structures commonly found in aeronautical applications like flapping-wing MAVs, in electronics cooling devices like piezoelectric fans (Kimber *et al.* 2007), and in biological structures like insect wings. Typically, the effect of the surrounding fluid is incorporated into the structural dynamics models by using experimentally measured fluid force data (Sarpkaya 1995). However, this approach is less effective when an *a priori* prediction of the structural amplitude response or an *a priori* estimate of the power consumption at resonance is required. Under these circumstances, a theoretical model which accounts *ab initio* for the effect of the surrounding fluid is more useful than a model which relies on the experimental fluid force data. In this article, we develop such a theoretical model for slender, sharp-edged *flexible* beams, which oscillate in a surrounding quiescent fluid at moderately high Reynolds numbers. Subsequently, we apply this theory to predict the *nonlinear, amplitude-dependent* damping of piezoelectric fans.

For small structural amplitudes, the vortex-shedding from the sharp edges of the structure can be neglected (Fu & Price 1987) and under these circumstances, the surrounding fluid gives rise only to an added-mass effect. Conversely, for large structural amplitudes, the vortices shed from the structure's sharp edges produce a damping effect on the structural oscillations (Sarpkaya 1995). In this article, we are concerned with this phenomenon of *vortex-shedding-induced* damping in slender, sharp-edged beams where the beam oscillation amplitudes are comparable to their widths. The focus is on developing experimentally validated theoretical models, which show the *amplitude* and *frequency* dependence of the *vortex-shedding-induced* aerodynamic damping.

Two non-dimensional parameters, namely, the Keulegan-Carpenter (KC) number and the frequency parameter β govern the phenomenon of *vortex-shedding-induced* damping for structures oscillating in a surrounding quiescent fluid (Keulegan & Carpenter 1958; Sarpkaya 1976). These parameters are defined as $KC = \frac{2\pi A}{c}$, and $\beta = \frac{c^2\omega}{2\pi\nu}$, where A is the structural amplitude, c is the characteristic length of the structure, ω is the angular frequency of structural oscillation and ν is the kinematic viscosity of the fluid. The Reynolds number for flows around such oscillating structures is the product of KC and β. In the current article, we study the aerodynamic damping of slender, sharp-edged beams for different values of KC and β. In particular, we present experimental results for the aerodynamic damping of piezoelectric fans, which are slender, sharp-edged beams with low KC numbers (ranging from 0 to 4) and moderately high values of β (ranging from 300 to 1200). Following these experimental results, we develop a theoretical

model that explains the *nonlinear* aerodynamic damping of slender, sharp-edged beams. The theoretical model is based on an inviscid fluid theory which *indirectly* accounts for the effects of viscosity by allowing vortex-shedding from the beam's sharp edges. Here, we point out that the direct numerical simulation approach used in a related work (Tao & Thiagarajan 2003) is computationally expensive when compared to the meshless boundary element solution presented in this article. We show that for slender, sharp-edged beams oscillating at amplitudes comparable to their widths, the essential features of the surrounding fluid flow and the aerodynamic forces can be captured by using an inviscid fluid theory with discrete vortex shedding from the beam's sharp edges.

The remainder of this article is arranged in the following fashion. In §2, we present experiments to demonstrate the phenomenon of nonlinear aerodynamic damping in slender, sharp-edged beams. In §3, we develop a theoretical model for predicting the nonlinear aerodynamic damping and the amplitude response of slender, sharp-edged beams. We compare the experimental results and the theoretical predictions in §4. Finally in §5, we summarize the findings of this work.

2. EXPERIMENTS

The main objective of the experiments is to measure the amplitude response of a slender, sharp-edged beam with the excitation frequency being incremented from a value below the resonant frequency to a value above the resonant frequency. From this amplitude response of the oscillating beam, the quality factor (Q-factor) of the frequency response can be extracted. Note that the Q-factor is specific to an eigen-mode and is equal to $1/(2\zeta_n)$, where ζ_n is the damping ratio of that eigen-mode. Experiments are performed both in vacuum and in air, to: (a) measure the natural frequency and estimate the structural damping of the beam in vacuum, (b) measure the *in-vacuo* mode shape and the mode shape in air, (c) estimate the combined structural and aerodynamic damping by oscillating the beam in air, and (d) estimate the modal forcing during the vacuum experiments. The set of measurements described above are repeated for increasing values of external excitation to capture the *nonlinear* behavior of the aerodynamic damping (Q-factor).

Piezoelectric fans are used for performing all the experiments. A piezoelectric fan consists of a piezoelectric patch bonded to a thin, flexible shim (made from either mylar or steel) as shown in figure 1. An applied time-varying voltage across the piezoelectric patch causes the transverse deflection (along the z-direction) of the shim. The experimental set-up is shown in figure 2. A piezoelectric fan (Piezo Systems, Inc.) was mounted inside a vacuum chamber (bell-jar with a vacuum pump) such that it can be viewed through a glass window. Three fans, fan 1 ($L_1 = 20.5$ mm, $L = 44.5$ mm, $c = 6.4$ mm, $t_b = 0.1$ mm, $t_p = 0.42$ mm), fan 2 ($L_1 = 22.9$ mm, $L = 44.1$ mm, $c = 12.7$ mm, $t_b = 0.1$ mm, $t_p = 0.4$ mm) and fan 3 ($L_1 = 28.3$ mm, $L = 64.9$ mm, $c = 12.6$ mm, $t_b = 0.25$ mm, $t_p = 0.55$ mm) were used for these experiments. A laser displacement sensor was used to measure the response amplitude at a single point (the black spot in figure 2a) on the fan. The mode shape of the fan was recorded by traversing the laser sensor along the axial direction. For the vacuum experiments, the absolute pressure in the chamber pressure was reduced to 10 Pa.

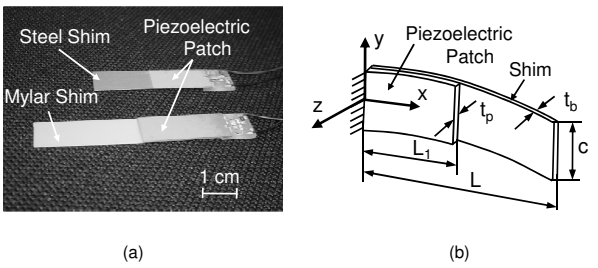

Figure 1: (a) Commercial piezoelectric fans, and (b) a schematic diagram of a piezoelectric fan.

In this article, we restrict our attention to studying the aerodynamic damping of piezoelectric fans oscillating in their first flexural mode. For fans 1 and 2, data were recorded for excitation frequencies ranging from 122 Hz to 134 Hz (with a 0.1 Hz increment) with applied voltage amplitude $\hat{V}$ ranging from 5 V to 25 V (with 5 V increments). These applied voltages gave rise to free-end oscillation amplitudes in the range of 1 mm to 5 mm, which are typical operating amplitudes for such fans. Similarly, for fan 3, the applied voltages $\hat{V}$ were 5 V, 15 V, 25 V, 40 V and 60 V with the excitation frequency ranging from 57 Hz to 63 Hz (with a 0.1 Hz increment).

The experimentally measured amplitude response of fan 3 *oscillating in air* is shown in figure 3; fans 1 and 2 show similar results. Each am-

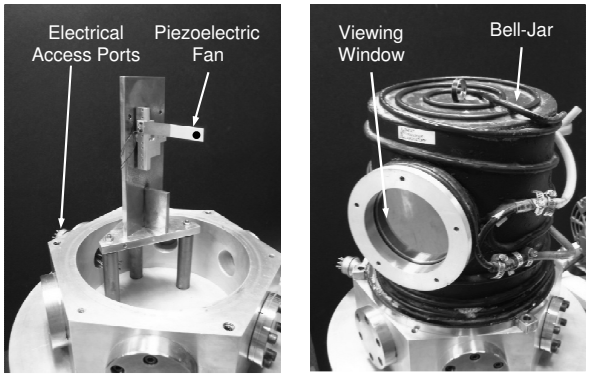

Figure 2: (a) A piezoelectric fan mounted inside the vacuum chamber, and (b) the vacuum chamber.

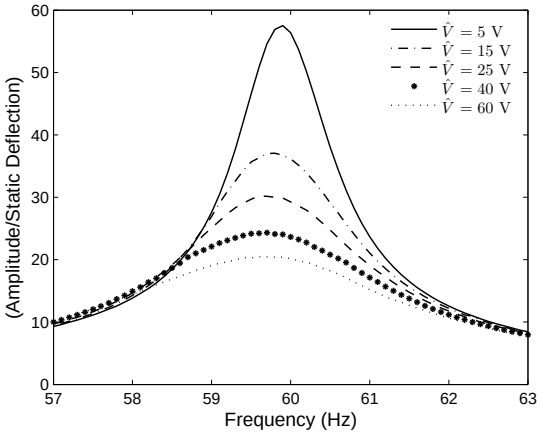

Figure 3: The normalized amplitude response of fan 3 for various applied voltages.

plitude response curve in figure 3 corresponds to a different value of applied voltage and is normalized such that *each curve has unit amplitude when the excitation frequency is zero.* We see that with increased fan oscillation amplitude, the *normalized* amplitude response curves become flatter, indicating an increased aerodynamic damping. The increase in damping is a purely aerodynamic phenomenon; an observation which was verified from the vacuum experiments where the damping remains unchanged even for increased fan oscillation amplitudes.

Using the Q-factors from the air and the vacuum experiments, we estimate the *aerodynamic* damping. The dependence of the aerodynamic damping (represented by the corresponding Q-factor) of the three fans on the KC number is shown in figure 4. The KC number in figure 4 is based on the free-end amplitude of the fan at the resonance frequency. The β value used in figure 4 for classifying the three fans is based on the resonant frequencies of the corresponding fans. Also, the data points shown in figure 4 represent the average values of the estimated quantities taken over a set of five experimental runs (the difference between the maximum and minimum values was less than 2%). From figure 4, we see that with increasing oscillation amplitude, the aerodynamic damping increases (or the Q-factor decreases) in a *nonlinear* fashion. In the next section, we develop a theoretical model that predicts and explains these trends.

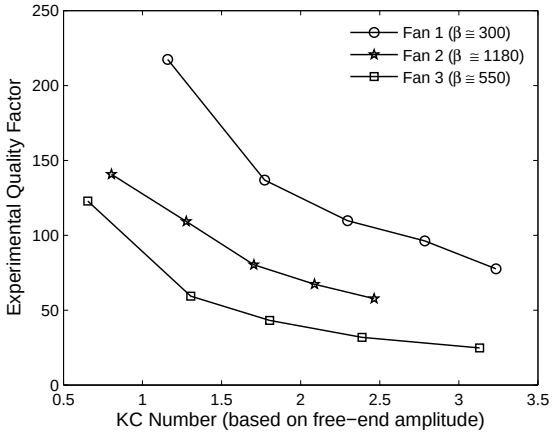

Figure 4: The variation of experimentally measured Q-factor with KC number for different fans.

3. THEORETICAL MODEL

The cantilever beam (see figure 5a) of width c and length L is modeled as a linearly elastic, isotropic Euler-Bernoulli beam. The displacement $w(x,t)$ of the beam is governed by:

$$\rho A_{cs} w_{,tt} + EI w_{,xxxx} = \Xi[w_{,tt}\,, w_{,t}\,] + F_{ext.}(x,t), \tag{1}$$

where ρ represents the density, A_{cs} represents the cross-sectional area, E represents the Young's modulus and I represents the moment of inertia of the beam. $\Xi[w_{,tt}\,, w_{,t}\,]$ is an operator which represents the fluid force per unit beam length and $F_{ext}(x,t)$ represents the externally applied force on the beam. The beam is assumed to be

clamped at $x = 0$ and free at $x = L$. It is assumed that the beam is surrounded by an initially quiescent, incompressible and inviscid fluid. For very large beam lengths (when $L \gg c$), it is sufficient to restrict the fluid flow problem in a two-dimensional plane parallel to the yz plane. The governing equation for the surrounding fluid flow is:

$$\bigtriangledown^2 \phi = 0, \tag{2}$$

where $\phi(y, z, t)$ is the velocity potential at a particular beam cross-section. The boundary condition for the fluid flow is obtained by matching the velocity of the beam with the normal velocity of the fluid on the surface of the beam. The singularities in the fluid flow solution at the sharp edges of the beam are removed by allowing separation at the beam's sharp edges through the application of the unsteady Kutta condition (Jones 2003). In the current article, the general solution to the fluid flow around a sharp-edged flat plate from the work of Jones (2003) will be adapted to the specific problem of an oscillating beam cross-section (see figure 5a).

Following the work of Jones (2003), a boundary integral method is used to express the complex velocity potential $\phi(\varsigma, t)$ (where $\varsigma = y + iz$) as a combination of the flow fields caused by a beam-bound vortex sheet and two free vortex sheets emanating from the sharp edges of the beam (See figure 5b). Then the velocity potential can be written as:

$$2\pi i \phi(\varsigma, t) = \begin{bmatrix} \int_{l_-(t)} \frac{\phi_-(\lambda,t)}{\lambda-\varsigma} d\lambda \ + \\ \int_{l_=(t)} \frac{\phi_=(\lambda,t)}{\lambda-\varsigma} d\lambda + \int_{l_+(t)} \frac{\phi_+(\lambda,t)}{\lambda-\varsigma} d\lambda \end{bmatrix}, \tag{3}$$

where, $l_=(t)$ represents the location of the beam-bound vortex sheet, and $l_-(t)$, $l_+(t)$ represent respectively, the locations of the free vortex sheets emanating from the two sharp edges of the beam cross-section. $\phi_-(\lambda, t)$, $\phi_+(\lambda, t)$ and $\phi_=(\lambda, t)$ represent the complex vortex sheet strengths associated with the vortex sheets $l_-(t)$, $l_+(t)$ and $l_=(t)$, respectively. Apart from the fluid boundary conditions mentioned above, it is required that the fluid flow perturbations caused by the beam motion are zero at large distances away from the beam and that the Kelvin circulation theorem is satisfied at every time instant. Requiring the flow velocities to remain finite at the two sharp edges of the beam cross-section results in the following

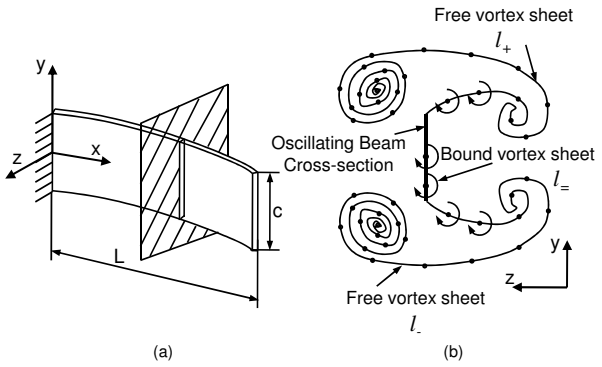

Figure 5: (a) A schematic diagram of a slender, sharp-edged cantilevered beam, and (b) a schematic diagram of the vortex shedding from the beam cross-section.

pair of equations:

$$2\pi w_{,t}(t) + \int_0^{\Gamma_+(t)} \Re\left(\frac{\sqrt{\zeta_+(\lambda,t) - \hat{c}_\mp}}{\sqrt{\zeta_+(\lambda,t) - \hat{c}_\pm}}\right) d\lambda - \int_0^{\Gamma_-(t)} \Re\left(\frac{\sqrt{\zeta_-(\lambda,t) - \hat{c}_\mp}}{\sqrt{\zeta_-(\lambda,t) - \hat{c}_\pm}}\right) d\lambda = 0, \tag{4}$$

where $w(t)$ is the displacement of the beam cross-section along the z-direction, and symbol $\Re$ denotes the real part of its argument. $\hat{c}_\pm = \pm\frac{c}{2}$ represents the two edges of the beam cross-section. $\Gamma_+(t)$ and $\Gamma_-(t)$ represent, respectively, the circulation around closed contours enclosing the free vortex sheets $l_+(t)$ and $l_-(t)$. Also, $\zeta_\pm(\Gamma, t)$ represents the position of the point on $l_\pm(t)$ at which the circulation is equal to $\Gamma(t)$. The two equations in equation (4) are solved simultaneously to obtain the value of the vorticity shed into the fluid flow at every time instant. The fluid force acting (in the z-direction) on the beam cross-section is $F(t) = -\int_{l_=(t)} p(\lambda, t) d\lambda$, where the expression for pressure $p(\lambda, t)$ is given in the work of Jones (2003).

The solution procedure described above is implemented using a C++ program and the results of this program were benchmarked against the work of Jones (2003). In figure 6, we present a set of representative results which were obtained after solving the fluid flow around a beam cross-section of width $c = 12.6$ mm undergoing the motion $w(t) = Acos(\omega t)$ (with $A = 1.26$ mm and $\omega = 118\pi$ rad/s) for a time period of $0.0285s$ (approximately 1.68 cycles). Figure 6a shows the free vortex sheets which have evolved from the beam's sharp edges and figure 6b shows the non-

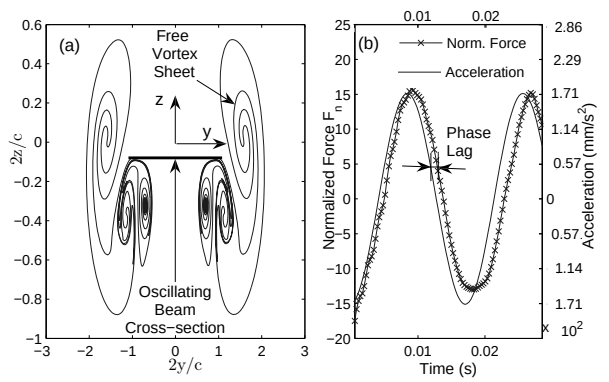

Figure 6: (a) Results of a representative computation showing the free vortex sheets shed from a beam cross-section, and (b) the computed force $F(t)$ and the acceleration of the beam cross-section.

dimensional normalized force $F_n = \frac{F(t)}{\rho_f (A\omega)^2 c}$ acting on the beam cross-section (where ρ_f is the fluid density) along with a plot of the beam acceleration $w_{,tt}(t)$. It is seen that the normalized force *lags* the beam acceleration by a small phase angle. This phase lag between the beam acceleration and the fluid force gives rise to the energy dissipation and is the main cause of the aerodynamic damping.

For low values of the KC number, the *periodic* force $F(t)$ can be approximated by the first harmonics of the Fourier series (Keulegan & Carpenter 1958), and this in turn leads to the following expression for $F(t)$:

$$F(t) = \rho_f A^2 \omega^2 c[A_1 cos(\omega t) + B_1 sin(\omega t)], \quad (5)$$

where A_1 and B_1 are the Fourier series coefficients. This description of the fluid force acting on a particular beam cross-section is coupled with the mode shape of the beam deflection, and after defining a *spatially dependent* Keulegan-Carpenter number as $KC(x) = \frac{2\pi \hat{A}_n \psi_n(x)}{c}$, from equation (5), we obtain an expression for the fluid force operator:

$$\Xi[w_{,tt}, w_{,t}] = -\rho_f \frac{KC(x)}{2\pi} c^2 A_1 w_{,tt} - \rho_f KC(x) \beta \nu B_1 w_{,t}. \quad (6)$$

The term $\rho_f \frac{KC(x)}{2\pi} c^2 A_1$ is the *amplitude-dependent* added-mass coefficient, while the term $\rho_f KC(x) \beta \nu B_1$ represents the *amplitude-dependent* aerodynamic damping. Substituting equation (6) into equation (1), we get:

$$\left\{ \rho A + \rho_f \frac{KC(x)}{2\pi} c^2 A_1 \right\} w_{,tt} + \{\rho_f KC(x) \beta \nu B_1 + \Lambda_{struct.}\} w_{,t} + EI w_{,xxxx} = F_{ext.}(x,t), \quad (7)$$

where the coefficient $\Lambda_{struct.}$ has been introduced to account for the structural damping. Equation (7) can be used for predicting *ab initio* the *nonlinear* aerodynamic damping and the amplitude response of slender, sharp-edged beams.

4. COMPARISON OF THEORY AND EXPERIMENT

Using a single-mode Galerkin approximation, from equation (7), we obtain:

$$M_s \ddot{q} + C_s \dot{q} + K_s q = -M_f \ddot{q} - C_f \dot{q} + F_{proj.}(t). \quad (8)$$

$M_f = \rho_f c^2 \int_0^L \frac{KC(x)}{2\pi} A_1 \psi^2(x) dx$ is the modal added mass and $C_f = \rho_f \beta \nu \int_0^L KC(x) B_1 \psi^2(x) dx$ is the modal aerodynamic damping, where $\psi(x)$ is the *in-vacuo* mode of the beam. Also, M_s, K_s, C_s, $F_{proj.}(t)$ represent respectively, the structural modal mass, structural modal stiffness, the structural modal damping and the modal forcing. Based on equation (8), the amplitude response $X_{air}(\omega)$ of the beam oscillating in air is given by:

$$X_{air}(\omega) = \frac{|F_{proj.}|}{\sqrt{(K_s - [M_s + M_f]\omega^2)^2 + ([C_s + C_f]\omega)^2}}. \quad (9)$$

Since the terms M_f and C_f depend on the magnitude of response $X_{air}(\omega)$, equation (9) needs to be solved iteratively in order to obtain $X_{air}(\omega)$. Equation (9) can be used to predict the amplitude response and the aerodynamic damping of a slender, sharp-edged beam. Next, we use equation (9) to compare the predictions of the theoretical model with the experimentally measured values of section §2.

For predicting the amplitude response of the piezoelectric fan oscillating in air, we use the following procedure. The data collected during the vacuum experiments are used for estimating the structural properties M_s, K_s, C_s and the modal forcing $|F_{proj.}|$ of the piezoelectric fan. These *experimentally estimated* structural properties and

the modal forcing are used along with the *theoretically predicted* aerodynamic forces for theoretically predicting the amplitude response of the fan.

Figure 7a shows a representative comparison of the *theoretically predicted* and the experimental amplitude response of fan 1 oscillating in air for an applied external voltage $\hat{V} = 5V$. It is seen that the error in predicting the resonant frequency is 0.28% and the error in predicting the peak amplitude is 7.94%. In figure 7b, we show a comparison of the experimentally estimated and the theoretically predicted aerodynamic Q-factors for the three fans. We see that the theoretical model predicts higher aerodynamic damping (lower Q-factors) when compared to the experimentally estimated Q-factors. The percentage error in predicting aerodynamic damping is approximately 15% or less for fans 1 and 3, while the percentage error for fan 2 is approximately 19% (this is attributed to the fact that fans 1 and 3 are more slender when compared to fan 2). Nevertheless, the theoretical model developed in this article is successful in capturing the trends of variation of the aerodynamic damping (or the Q-factor) with increasing oscillation amplitude (or the KC number). The vortices shed at a particular beam cross-section are constrained to remain in that plane and subsequently lead to larger fluid forces that cause an over-prediction of the aerodynamic damping. The utility of the model developed here lies in the fact that the model uses an inviscid fluid flow theory (with the advantage of less computational effort), and yet is able to capture the nonlinear trends in the aerodynamic damping with approximately 15% error when compared to the experimental values.

5. CONCLUSIONS

In this article, we address the general problem of slender, sharp-edged beams oscillating in surrounding air at moderately high Reynolds numbers by focusing on the specific case of piezoelectric fans. Experiments were used to demonstrate the phenomenon of *amplitude-dependent* aerodynamic damping in piezoelectric fans. A *first-principles* theoretical model which incorporated the two non-dimensional parameters KC and β was developed to explain the nonlinear aerodynamics of slender, sharp-edged beams oscillating at moderately high Reynolds numbers. The theoretical model successfully predicted the nonlinear trends of aerodynamic damping approximately to within 15% of the experimental values.

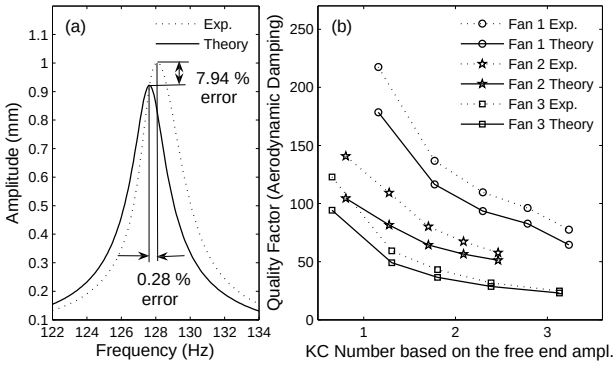

Figure 7: (a) Comparison of the theoretical and experimental amplitude response, and (b) comparison of the theoretical and the experimental Q-factors.

6. REFERENCES

Fu, Y. & Price, W. G. 1987 *Interactions between a partially or totally immersed vibrating cantilever plate and the surrounding fluid. J. Sound Vib.* **118**(**3**), 495–513.

Jones, M. A. 2003 *The separated flow of an inviscid fluid around a moving flat plate. J. Fluid Mech.* **496**, 405–441.

Keulegan, G. H. & Carpenter, L. H. 1958 *Forces on cylinders and plates in an oscillating fluid. J. Res. Nat. Bur. Stand.* **60**(**5**), 423–440.

Kimber, L., Garimella, S. V. & Raman, A. 2007 *Local heat transfer coefficients induced by piezoelectrically actuated vibrating cantilevers. J. Heat Trans.-ASME* **129**, 1168–1176.

Sarpkaya, T. 1976 Vortex shedding and resistance in harmonic flow about smooth and rough circular cylinders at high Reynolds numbers. Technical report no. NPS-59SL76021, Naval Postgraduate School, CA, USA.

Sarpkaya, T. 1995 *Hydrodynamic damping, flow-induced oscillations, and biharmonic response. J. Offshore Mech. Arct.* **117**, 232–238.

Tao, L. & Thiagarajan, K. 2003 *Low KC flow regimes of oscillating sharp edges I. Vortex shedding observation. Appl. Ocean Res.* **25**, 21–35.